BMC Cancer

RESEARCH Open Access

Niosomal mefloquine and cisplatin in breast cancer: comparative effects on apoptosis and angiogenesis via in vitro and in silico analysis

Zohreh Salari[1], Ahmad Khosravi[2*], Arezo Riahi[1*], Elaheh Molaakbari[2], Ehsan Salarkia[2], Ali Reza Keyhani[2], Samira Sohbati[1], Ghazal Mansouri[1], Mina Khosravi[3], Mohammad Zarif[2] and Mohammad Amin Raeisi Estabragh[4]

Abstract

Background Breast cancer remains a leading cause of cancer-related death among females, with triple-negative breast cancer (TNBC) posing significant therapeutic challenges due to its aggressive behavior and lack of targeted treatments. Mefloquine (MEF), an antimalarial agent, exhibits anticancer activity by disrupting lysosomal function and enhancing ROS-mediated apoptosis. Cisplatin (CIS) induces apoptosis but is limited by drug resistance. This study investigates the combined effects of MEF, in both free and niosomal forms, and CIS on apoptosis and angiogenesis in breast cancer cells.

Methods The cytotoxicity of MEF, CIS, and their combinations was assessed in MCF-7 and TNBC cell lines using MTT assays. Gene expression and ELISA analysis confirmed significant upregulation of pro-apoptotic markers *Bax* ($p < 0.001$) and *CASP3* ($p < 0.001$), and downregulation of anti-apoptotic Bcl-2 ($p < 0.001$) and angiogenic factors *VEGF* and *KDR*. Molecular docking studies (Molegro Virtual Docker) evaluated binding affinities of MEF and CIS to BAX, Bcl-2, and VEGFR. NMEF was prepared and characterized for stability and encapsulation efficiency.

Results NMEF demonstrated high encapsulation efficiency (87.21%) and was stable over six months. Combination treatments, particularly Cisplatin-niosomal Mefloquine (CIS-NMEF), showed synergistic cytotoxicity (CI < 1) and significantly lower IC50 values in both cell lines (TNBC: 2.30 µg/ml). Molecular docking revealed strong binding affinities for CIS-NMEF with BAX (-139.72), Bcl-2 (-136.09), and VEGFR (-139.19). Gene expression analysis confirmed upregulation of pro-apoptotic markers (*Bax*, *CASP3*) and downregulation of anti-apoptotic *Bcl-2* and angiogenic factors (*VEGF*, *KDR*). ROS production increased significantly in combination groups, indicating enhanced oxidative stress.

*Correspondence:
Ahmad Khosravi
khosraviam@yahoo.com
Arezo Riahi
riahiarezoo2@gmail.com

Full list of author information is available at the end of the article

Conclusion The niosomal formulation of MEF synergistically enhances CIS efficacy by promoting apoptosis, and suppressing angiogenesis in TNBC. These findings highlight NMEF as a promising chemosensitizer to overcome cisplatin resistance. Future studies should focus on in vivo validation and clinical translation.

Keywords Mefloquine, Cisplatin, Breast cancer, Apoptosis, Angiogenesis

Introduction

Breast cancer ranks as the second leading cause of cancer-related mortality among females in the United States as of 2023. Globally, it represents a significant public health concern and is the most frequently diagnosed malignant disease in females [1]. Around 30% of women first diagnosed with early-stage breast cancer later develop metastases, reducing the five-year survival rate from 85 to 99% to roughly 25% and the average survival to about two years [2]. Triple-negative breast cancer (TNBC) represents 10–20% of invasive cases and lacks estrogen, progesterone, and HER2 receptors. Compared with other subtypes, it carries a greater risk of recurrence and metastasis [3].

Apoptosis, a programmed cell death process, maintains cellular homeostasis by eliminating damaged or excess cells. It operates through intrinsic (mitochondrial) and extrinsic (death receptor) pathways regulated by pro-apoptotic proteins like Bax and caspases and anti-apoptotic proteins such as Bcl-2 [4, 5]. Therapies that enhance pro-apoptotic signaling can restore chemotherapy sensitivity and induce tumor regression by shifting the Bax/Bcl-2 ratio toward apoptosis [6].

Angiogenesis, the formation of new blood vessels, is essential for tumor growth and metastasis by providing oxygen and nutrients to cancerous tissues. This process is primarily driven by vascular endothelial growth factor (VEGF) and its receptor VEGFR (KDR), which are frequently overexpressed in aggressive tumors like TNBC, leading to poor prognosis and therapy resistance. Inhibiting VEGF/VEGFR-mediated angiogenesis disrupts tumor vascularization, restricts metastasis, and improves drug delivery and treatment efficacy. Thus, combining pro-apoptotic and anti-angiogenic strategies offers a complementary and potent approach for breast cancer therapy [6, 7].

Cisplatin (CIS), a first-line platinum-based chemotherapeutic, induces apoptosis through DNA cross-linking. However, its effectiveness is often reduced by acquired resistance, a major challenge in breast cancer treatment. This study explores a combination strategy, proposing that agents with different mechanisms—cisplatin targeting DNA and mefloquine affecting lysosomal and mitochondrial pathways, may act synergistically to overcome resistance [8]. CIS promotes apoptosis via mitochondrial pathways and inhibits angiogenesis by reducing the expression of VEGF and HIF-1α in tumor cells [9]. The drug's clinical utility, however, is frequently limited by the development of resistance. Key cellular resistance mechanisms to CIS include: (i) reduced intracellular drug accumulation through decreased uptake or increased efflux, (ii) enhanced detoxification by thiol-containing molecules like glutathione, (iii) improved DNA damage repair capacity, and (iv) evasion of apoptosis [8, 10]. These resistance pathways, often mediated through membrane glycoproteins and DNA repair enzymes, represent major obstacles in breast cancer treatment [11]. Additionally, lysosome-mediated processes, such as autophagy, contribute to chemoresistance by enabling cancer cells to survive CIS-induced stress [12].

Mefloquine (MEF), a quinoline-based antimalarial, has been clinically used for malaria prophylaxis for over three decades [13]. Structurally, it is a chiral molecule containing two chiral centers. Its mechanism involves inhibiting protein synthesis via interaction with the 80 S ribosomal GTPase of *Plasmodium falciparum* [14, 15]. At the cellular level, MEF targets lysosomes, reducing tumor invasiveness, angiogenesis, and progression. It increases lysosomal membrane permeability, leading to cathepsin release into the cytosol [16], and induces mitochondrial oxidative stress by upregulating superoxide dismutase [17]. MEF hyperpolarizes the mitochondrial membrane potential, elevates Reactive Oxygen Species (ROS) production, and reduces ATP synthesis [18, 19]. Molecularly, it inhibits PI3K/Akt and mTOR phosphorylation while activating JNK, ERK, and AMPK cascades [20]. In colorectal cancer cells, MEF suppresses nuclear factor kappa B (NF-κB) signaling and induces apoptosis [21]. Similarly, MEF induces apoptosis in breast cancer cells by increasing ROS production, disrupting lysosomal function, and activating caspase-3 while downregulating Bcl-2 expression [22]. Additionally, MEF exhibits anti-angiogenic effects by impairing VEGF signaling and endothelial tube formation, as demonstrated in glioblastoma models [16].

Novel lipid-based drug delivery systems, such as niosomes, have been increasingly utilized for the delivery of various drugs, including anticancer medications [23]. Niosomes, made of non-ionic surfactants and cholesterol, can encapsulate both lipophilic and hydrophilic drugs, enhancing efficacy while minimizing side effects [24]. Niosomes can be produced by various methods, with microfluidics being a recent approach that generates monodisperse niosomes at the nanometer scale in a single step [25, 26].

Combining antimalarials with platinum-based chemotherapy shows promise in various cancers, especially breast and prostate. Although mechanisms differ by drug and cancer type, synergy may improve outcomes, overcome resistance, and reduce side effects. This study evaluates a combined MEF and CIS therapy (CIS-MEF) and a niosomal formulation (CIS-NMEF) to enhance delivery and bioavailability in breast cancer. Using MCF7 and TNBC cell lines, we assess cellular responses, viability, treatment efficacy, and molecular signaling to better understand heterogeneity and resistance.

Materials and methods

In silico modeling

For docking studies, CIS, MEF, CIS-MEF, and CIS-NMEF were evaluated using Molegro Virtual Docker (MVD) [1]. CIS and MEF were docked individually to assess their independent interactions with BAX (PDB: 5W5X), Bcl-2 (PDB: 5JSN), and VEGFR (PDB: 4KZN). For CIS-MEF, simultaneous docking was performed with CIS and MEF as separate ligands to explore cooperative interactions, inspired by Multiple Ligand Simultaneous Docking (MLSD) approaches [2]. The 3D structures of CIS and MEF were obtained from PubChem as SDF files, optimized using HyperChem with the MM + force field and AM1 semi-empirical method, and docked using MVD's MolDock SE algorithm with a grid resolution of 0.3 Å [27]. For CIS-NMEF, CIS was docked as a separate ligand in the presence of NMEF, which was modeled as a niosomal structure encapsulating MEF, based on in vitro results showing enhanced efficacy of the niosomal formulation. Subsequently, molecular quantum design for the NMEF was carried out using the DMol3 module within Materials Studio [28]. This included comprehensive energy calculations for the Highest Occupied Molecular Orbital (HOMO) and Lowest Unoccupied Molecular Orbital (LUMO) levels. The most stable configuration was identified and saved in SDF format for future reference. Fig. 1 illustrate the NMEF structure that was prepared for molecular docking studies.

In vitro examination

Materials and reagents

Cisplatin (Sigma-Aldrich, Catalog #: 1134357), Mefloquine hydrochloride (MedChemExpress, Catalog #: HY-13628), Span 60 (Sigma-Aldrich, Catalog #: 85548), Tween 60 (Sigma-Aldrich, Catalog #: 93743), Cholesterol (Sigma-Aldrich, Catalog #: 110423), DMEM (Gibco, Catalog #: 10569044), Fetal Bovine Serum (FBS) (Gibco, Catalog #: 10270106), MTT reagent (Merck, Catalog #: 11544457001), ELISA kits for Bax (MyBioSource, Catalog #: MBS935667), Bcl-2 (MyBioSource, Catalog #: MBS9501407), CASP3 (MyBioSource, Catalog #: MBS040290), VEGF, and KDR.

Niosomal drug Preparation

Niosomal formulation of MEF was prepared using the microfluidic method [26]. Briefly stock solutions of non-ionic surfactants (Span 60®, and Tween 60®,) cholesterol, and MEF hydrochloride were prepared in ethanol. A lipid phase (comprising surfactants, cholesterol, and the drug) and phosphate-buffered saline (PBS) were introduced into a microchannel system (Nanosynthesizer Insight™, Iran) as the organic and aqueous phases, respectively. Mixing was achieved using syringe pumps at an aqueous-to-organic flow rate ratio (FRR) of 1:5 and a total flow rate (TFR) of 12 ml/min at 55 °C. After preparation, the formulation was dialyzed (Visking tube, MW cut off 12 KD) against 100 mL of PBS for 4 h to remove free drug and ethanol.

Vesicle size (Z-average) and polydispersity index (PDI) were determined by dynamic laser light scattering (Cordouan VASCO™, France). The physical stability of niosomes stored at 4–8 °C was evaluated by measuring size at one week, one month, 3, and 6 months [23]. The encapsulation efficiency (EE) of MEF in the niosomes was determined by disrupting the niosomal bilayers with 1 mL isopropyl alcohol. The amount of encapsulated drug was then measured using a previously established method [29].

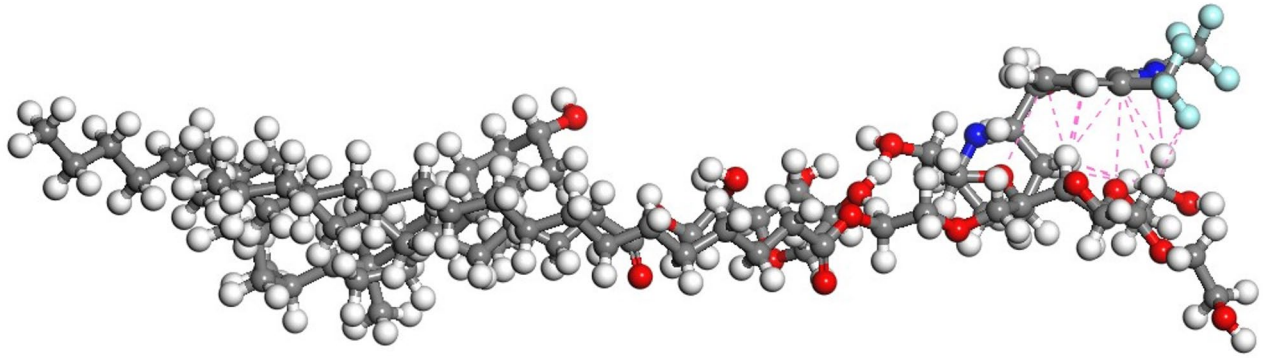

Fig. 1 Molecular structure designed of NMEF by Materials Studio software

For the combination treatment groups, the NMEF formulation was first prepared according to the protocol described above. Subsequently, a stock solution of CIS was added to the MEF and NMEF suspension in ratio 1:1 to achieve the desired final concentrations of each drug for cell treatment. This combination was used as the CIS + MEF and CIS + NMEF treatment group in the experiments.

Cell culturing

The MCF-7 cell line and the triple-negative breast cancer (ATCC HTB-22) cell line MDA-MB-231 (ATCC HTB-26) were obtained from the Pasteur Institute of Iran, were transferred into Dulbecco's Modified Eagle Medium (DMEM) (Gibco, USA) supplemented with 0.5% fom 80 mg/ml gentamicin and 15% fetal bovine serum (FBS) (Gibco, USA). The cultures were then maintained in a humidified atmosphere with 5% CO_2 at 37 °C.

Cytotoxicity tests

The flasks were removed from the incubator, and after washing with PBS solution, adherent cells covering the flask surface were detached using trypsin. Following centrifugation, the supernatant was discarded, and the cell pellet was resuspended in complete culture medium. The cells were then thoroughly mixed and seeded into cell culture plates. To determine cell viability, a trypan blue exclusion assay was performed. Cells were mixed with 0.4% trypan blue solution in a 1:1 ratio, and the mixture was carefully loaded into a hemocytometer (Neubauer chamber) for cell counting. Approximately 1×10^3 cells per well were seeded into a 96-well plate.

CIS was added at concentrations of 1.25, 2.5, 5, 10, and 20 µg/mL in triplicate. Similarly, MEF was tested at the same concentrations. Additionally, a combination of CIS and MEF (CIS-MEF) (at identical concentrations) was evaluated. These treatments were performed separately for MCF7 and TNBC cell lines (obtained from the Pasteur Institute of Iran) in independent plates. The plates were incubated for 24 h in a 5% CO_2 incubator at 37 °C. The concentrations for the combination studies were selected based on a fixed-ratio design derived from the IC50 values of each individual drug.

The MTT assay is based on the reduction of yellow tetrazolium salt (MTT) to purple formazan crystals by mitochondrial succinate dehydrogenase in viable cells. The intensity of the color correlates with cell viability. After 24 h of drug exposure, 10 µg of MTT solution (5 mg/mL, Merck, Germany) was added to each well, followed by 4 h of incubation at 37 °C. The plates were then centrifuged, and the supernatant was removed. Next, 100 µL of isopropanol was added to each well to solubilize the formazan crystals. The plates were kept in the dark at room temperature for 1 h. The optical density (OD) was measured at 570 nm using an ELISA reader (BioTek ELX800, USA). Cell viability percentages were calculated for each concentration. All steps were performed separately for both cell lines. Cell viability percentage was calculated using the formula (OD_sample/OD_control) × 100. The IC50 values (the concentration that inhibits 50% of cell growth) were then determined using non-linear regression analysis in GraphPad Prism software (Version 10.0). To evaluate the drug interactions, the Combination Index (CI) was calculated using the Chou-Talalay method. According to this method, CI values of <1, $=1$, and >1 were interpreted as synergistic, additive, and antagonistic effects, respectively.

Table 1 The list of primers

Gene	Forward sequence (5′–3′)	Reverse sequence (5′–3′)	Product size (bp)
Bax	CCCGAGAGGTCTTTTTCCGAG	CCAGCCCATGATGGTTCTGAT	155
Bcl-2	GGTGGGGTCATGTGTGTGG	CGGTTCAGGTACTCAGTCATCC	89
CASP3	CATGGAAGCGAATCAATGGACT	CTGTACCAGACCGAGATGTCA	59
CASP7	AGAGTCTGTGCCCAAATCAAC	CTGCTTCTCTCTTTGCTGAA	59
GAPDH	CCTCTCTGGCAAAGTCCAAG	GGTCACGCTCCTGGAAGATA	176
KDR	GCCAACTCTATGGCAGAAGC	CTGAACACCATGCCACTGTC	86
VEGF-A	CAATTGAGACCCTGGTGGAC	TCTCATCAGAGGCACACAGG	86

Measurement of gene expression

Total cellular RNA was extracted using the Acid Guanidinium Thiocyanate-Phenol method (Roche) according to the manufacturer's protocol. For cDNA synthesis, 1 µg of the extracted RNA was reverse-transcribed using a cDNA synthesis kit (Yekta Tajhiz Co.) following the recommended procedure. Gene expression analysis was performed using quantitative real-time PCR (qPCR) to evaluate the mRNA levels of apoptosis-related genes (*BAX*, *BCL2*, *CASPASE 3*, and *CASPASE 7*) and angiogenesis-related genes (*VEGF* and *KDR*), with GAPDH serving as the reference gene. Specific primers listed in the designated table were used for amplification. The reaction mixture was prepared according to Table 1, including positive and negative controls, and loaded into a Rotor-Gene Q real-time PCR cycler (QIAGEN). The qPCR reactions were performed in a final volume of 20 µL. Each reaction mixture contained 10 µL of SYBR Green master mix, 2 µL of cDNA template, 1 µL of each forward and reverse primer (at a concentration of 10 pmol/µL), and nuclease-free water to reach the final volume. The thermal cycling protocol followed the time and

temperature conditions outlined in Table 1. Relative gene expression levels were quantified using the comparative Ct method ($2^{-\Delta\Delta Ct}$), with data normalized to GAPDH and compared to untreated controls.

ELISA assay

To quantify the levels of angiogenetic and apoptotic mediators, supernatants were collected from treated and untreated cell culture wells and subjected to enzyme-linked immunosorbent assays (ELISA). Specifically, Apoptotic mediators, including CASP3 (MBS040290), CASP8 (MBS260539)Bax (MBS935667), and Bcl-2 (MBS9501407), and angiogenetic mediators including KDR and VEGF were quantified using ELISA kits (MyBioSource, USA). All assays were performed according to the manufacturer's protocols.

ROS production

To measure the average ROS production on the treated MCF7 and TNBC cell lines. The cells were treated for 48 h. Intracellular ROS levels were measured using the fluorescent dye 2',7'-dichlorofluorescin diacetate (DCFH-DA). After treating the cells for 48 h, they were washed with PBS and then incubated with 10 µM of DCFH-DA in serum-free medium for 30 min at 37 °C in the dark. Following incubation, the cells were washed again with PBS to remove the excess dye. The fluorescence intensity, which corresponds to the level of intracellular ROS, was then measured using a Marshall Scientific BD Bioscience FacsCanto II Flow Cytometer, and data were analyzed using Flowjo software (Version 10.0).

Statistical analysis

The statistical analysis was conducted using SPSS version 22 and GraphPad Prism version 10.0. Data were presented as mean ± standard deviation (SD) for continuous variables. To compare the differences between groups, a one-way analysis of variance (ANOVA) followed by Tukey's post-hoc test was employed for multiple comparisons. For pairwise comparisons, an independent samples t-test was used. The significance level was set at $^{*}p^{*} < 0.05$ for all tests.

Results

In silico

MVD molecular Docking

To validate the docking protocol, the co-crystallized ligands from the PDB structures of BAX (5W5X), Bcl-2 (5JSN), and VEGFR (4KZN) were re-docked into their respective binding sites using Molegro Virtual Docker (MVD). The root-mean-square deviation (RMSD) between the re-docked and native poses was calculated to ensure accuracy. RMSD values were < 2 Å for all targets (BAX: 1.45 Å; Bcl-2: 1.62 Å; VEGFR: 1.73 Å), confirming that the docking protocol reliably reproduced the native binding configurations. This validation step ensured the robustness of the docking results for CIS, MEF, CIS-MEF, and NCIS-MEF.

Table 2 Calculated Docking score by MVD

Compound	CIS	MEF	CIS-MEF	CIS-NMEF
BAX	−46.19	−88.43	−152.69	-−147.05
Bcl-2	−48.96	−79.44	−130.14	−134.89
VEGFR	−52.68	−74.23	−122.68	−147.98

The binding energies of CIS, MEF, CIS-MEF, and CIS-NMEF with BAX (PDB: 5W5X), Bcl-2 (PDB: 5JSN), and VEGFR (PDB: 4KZN) were evaluated using Molegro Virtual Docker (MVD). The docking results are summarized in Table 2, with negative MolDock scores indicating spontaneous ligand-receptor interactions. For CIS-MEF, simultaneous docking of CIS and MEF as separate ligands was performed to explore cooperative interactions. The results showed enhanced binding affinities, suggesting synergistic interactions. For CIS-NMEF, CIS was docked as a separate ligand in the presence of NMEF, reflecting the in vitro co-administration setup. The results confirm enhanced binding, consistent with the in vitro synergy observed with the niosomal formulation. Binding analyses (Figs. 2, 3 and 4) show specific interactions with key amino acids, supporting the cooperative binding of CIS and MEF..

Molecular docking results for CIS, MEF, CIS-MEF, and CIS-NMEF with BAX, Bcl-2, and VEGFR receptors were evaluated in terms of binding energy. MolDock scores reflect the binding probabilities of the compounds. Negative energy values indicate spontaneous ligand-receptor interactions. Table 2 presents the binding configurations of the compounds along with their respective parameters. The MolDock scores for the molecular binding of CIS, MEF, CIS-MEF, and CIS-NMEF with BAX were – 46.19, –88.43, –152.69, and – 147.05, respectively.

Figure 2 illustrates the molecular binding results of CIS, MEF, their free combination, and niosomal form with the receptor PDB ID: 5W5X (related to BAX). Binding analysis revealed that CIS interacts with BAX through amino acids Asp(A)33 and Glu(A)41 (Fig. 2A). Additionally, MEF interacts with BAX at a binding site involving amino acid Gln(A)77, Ile(A)80, Ala(A)81, Val(A)83, Thr(A)85, Lys(A)119, leu(A)120, and Lys(A)123 (Fig. 2B). Binding analysis in Fig. 2C shows that the free CIS-MEF forms bonds with BAX using amino acids Asp(A)33, Glu(A)41, Ile(A)80, Ala(A)81, Val(A)83, Thr(A)85, Lys(A)119, leu(A)120, and Lys(A)123. Furthermore, as shown in Fig. 2D, the CIS-NMEF is stabilized by BAX through amino acids Gln(A)32, Asp(A)33, Arg(A)34, Ala(A)35, Gly(A)36, Arg(A)37, and Glu(A)41.

The exciting findings from our study reveal the MolDock scores for the molecular binding of CIS, MEF,

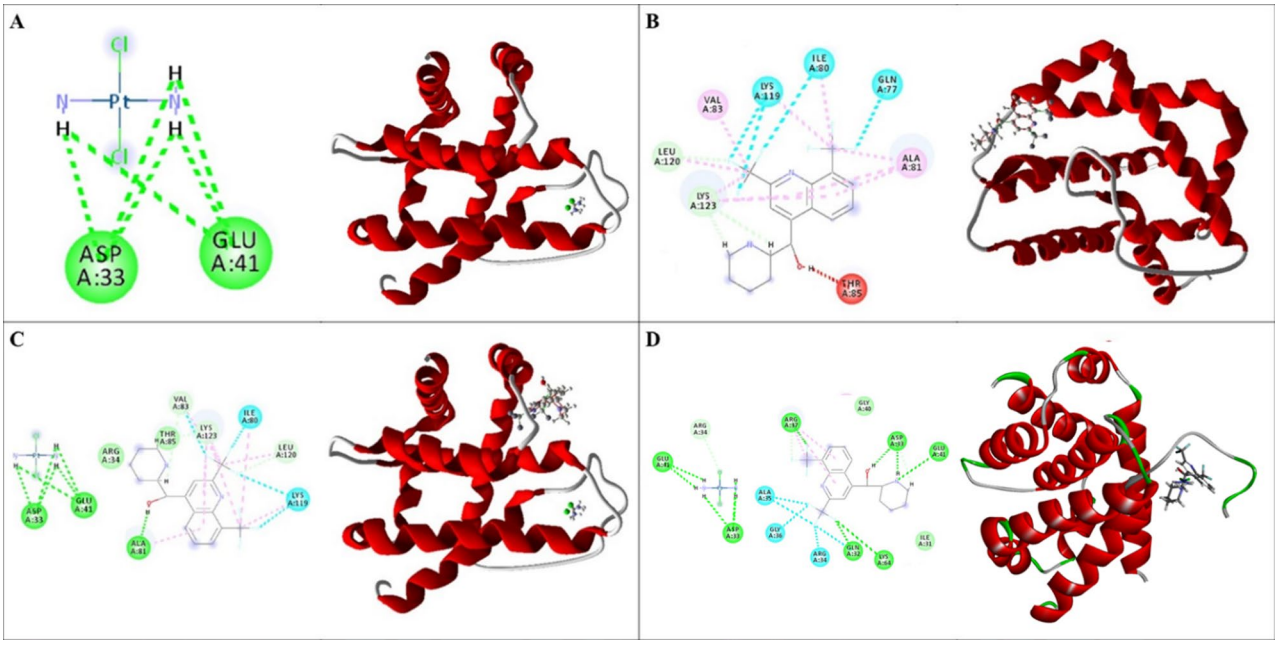

Fig. 2 Illustration of the best docking score solution for BAX (utilizing the chosen crystal structure of 5W5X) with (**A**) CIS, (**B**) MEF, (**C**) CIS-MEF and (**D**) CIS-NMEF along with the ligand mapping depicting various chemical bonds in Discovery Studio

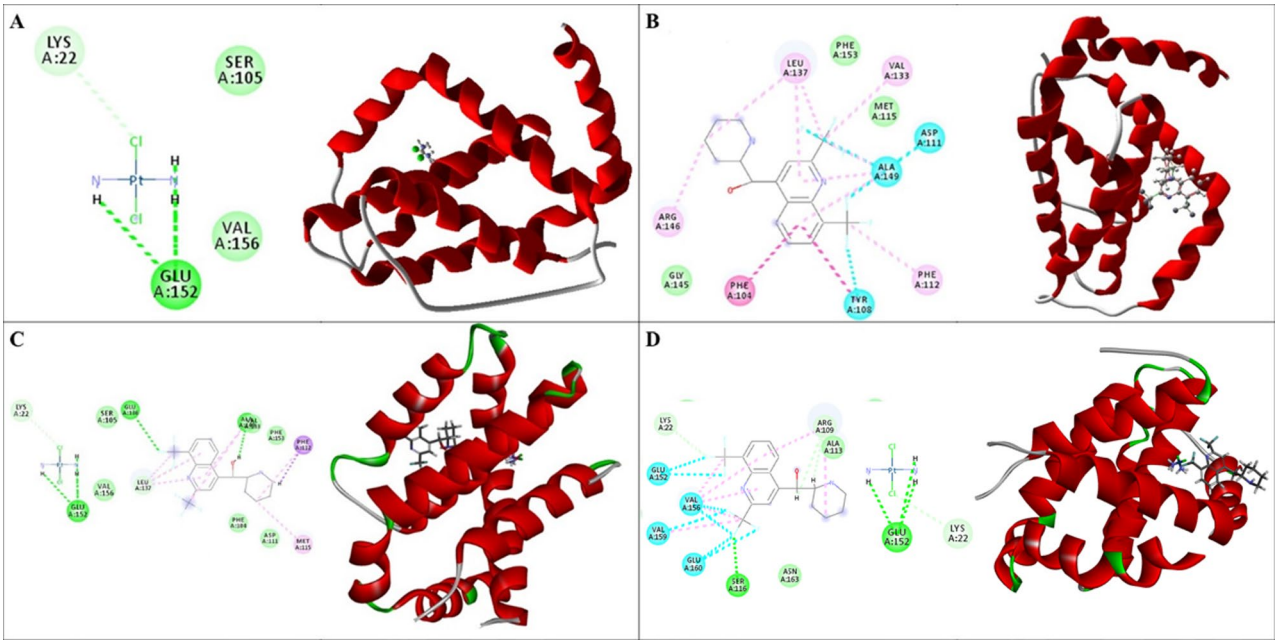

Fig. 3 Illustration of the best docking score solution for Bcl-2 (utilizing the chosen crystal structure of 5JSN) with (**A**) CIS, (**B**) MEF, (**C**) CIS-MEF, and (**D**) CIS-NMEF along with the ligand mapping depicting various chemical bonds in Discovery Studio

CIS-MEF, and CIS-NMEF with the protein Bcl-2, which are −48.96, −79.44, −130.14, and −134.89, respectively. These Fig.s illustrate the intricate molecular interactions of CIS, MEF, their combination, and the niosomal form with Bcl-2, as identified by PDB ID: 5JSN.

Upon closer examination of the binding analysis, we observe that CIS forms crucial interactions with Bcl-2 through the amino acids Lys(A)22 and Glu(A)159, as illustrated in Fig. 3A. Meanwhile, MEF uniquely engages with Bcl-2 at a specific site involving the amino acid Phe(A)104, Tyr(A)108, Asp(A)111, Phe(A)112, Val(A)133, Leu(A)137, and Ala(A)149, depicted in Fig. 3B. In Fig. 3C, the free combination of CIS and MEF demonstrates its ability to establish a robust connection

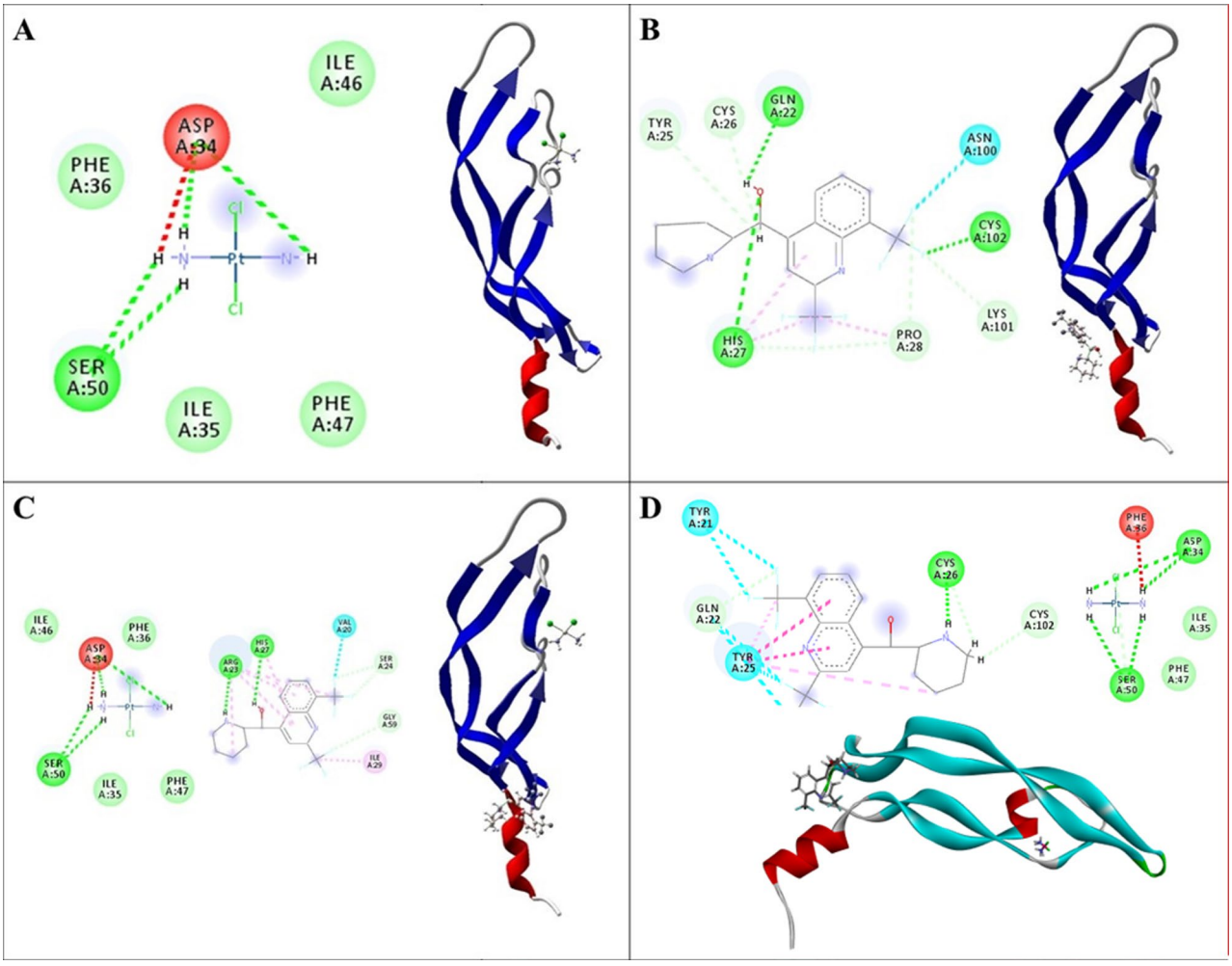

Fig. 4 Illustration of the best docking score solution for VEGFR (utilizing the chosen crystal structure of 4KZN) with (**A**) CIS, (**B**) MEF, (**C**) CIS-MEF, and (**D**) CIS-NMEF along with the ligand mapping depicting various chemical bonds in Discovery Studio

with Bcl-2 utilizing the amino acids Lys(A)22, Phe(A)112, Met(A)115, Val(A)133, Glu(A)136, Leu(A)137, Ala(A)149 and Glu(A)159. Lastly, our findings indicate that CIS-NMEF finds stability through interactions with Bcl-2, specifically via amino acids Lys(A)22, Arg(A)109, Ala(A)113, Ser(A)116, Glu(A)152, Val(A)156, Val(A)159 and Glu(A)160, showcasing yet another layer of complexity in these molecular interactions. These insights highlight the individual contributions of each compound and emphasize the dynamic nature of their collaborative binding with Bcl-2.

Additionally, the MolDock scores for CIS, MEF, CIS-MEF, and CIS-NMEF binding with VEGFR were −52.68, −74.23, −122.68, and −147.98, respectively. Figure 4 displays the ligand interaction maps and molecular binding configurations of CIS, MEF, their free combination, and niosomal form with the receptor 4KZN (PDB ID for VEGFR). Binding analysis indicated molecular interactions between CIS and VEGFR through specific amino acids Asp(A)34, and Ser(A)50 (Fig. 4A). MEF also interacts with VEGFR via amino acid Gln(A)22, Tyr(A)25, Cys(A)26, His(A)27, Pro(A)28, Asn(A)100, Lys(A)101 and Cys(A)102 (Fig. 4B). Binding analysis in Fig. 4C shows interactions between the free CIS-MEF and VEGFR amino acids Val(A)20, Arg(A)23, Ser(A)24, His(A)27, Ile(A)29, Glu(A)30, Asp(A)34, Ser(A)50 and Gly(A)59. The CIS-NMEF interacts with VEGFR amino acids Tyr(A)21, Gln(A)22, Tyr(A)25, Cys(A)26, Asp(A)34, Phe(A)36, Ser(A)50 and Cys(A)102, as observed in Fig. 4D.

The results from molecular docking studies revealed that both MEF and CIS exhibit significant binding affinity for the receptors BAX, Bcl-2, and VEGFR, as indicated by their respective MolDock scores (Table 2). Notably, MEF exhibited a more robust binding interaction with both BAX and Bcl-2, as well as VEGFR, compared to CIS, suggesting a stronger affinity for these targets. Furthermore, when assessing the therapeutic potential of the two compounds in combination, both free and niosomal formulations of MEF and CIS demonstrated improved binding affinity scores. This enhanced binding suggests a synergistic effect between MEF and CIS, which could

potentially lead to increased efficacy in therapeutic applications aimed at modulating the activity of these key receptors involved in angiogenesis and autophagy. BAX, Bcl-2, and VEGFR.

In vitro

Niosomal drug preparation

A niosomal formulation was studied using the dynamic light scattering method. The Z-average diameter of the formulation is 218.02 ± 5.1 nm (PDI: 0.277) initially, and the formulation maintained physical stability over six months at 4 °C, with final sizes of 251.06 ± 4.8 nm (PDI: 0.221). Also, the vesicle size distribution of the formulations had a normal bell-shaped curve (Fig. 5). Standard calibration curves for drug quantification were established using UV-Vis spectrophotometry, with a maximum absorption at 280 nm. Encapsulation efficiency reached 87.21 ± 1.30% for MEF (Table 3).

Cytotoxicity

The cytotoxic effects of various concentrations of MEF (in both free and niosomal forms), CIS, and their combinations were evaluated on MCF-7 and TNBC cell lines, as illustrated in Fig. 6. The half-maximal inhibitory concentrations (IC50) for each treatment are detailed in Table 4. The selective index (SI) was calculated to compare the cytotoxicity between the highly aggressive TNBC cell line and the less aggressive MCF-7 cell line, as a normal breast cell line was not used in this study. An SI value greater than 1 suggests that the treatment is selectively more toxic to the aggressive TNBC cells. As detailed in Table 4, the SI values for all treatments exceeded 1. Furthermore, analysis of drug synergy revealed that combining MEF (both free and niosomal forms) with CIS resulted in a synergistic effect (Combination Index, CI < 1) in both cell lines. Specifically, in MCF-7 cells, the CI values were 0.892 for the free MEF and CIS combination and 0.883 for the niosomal MEF and CIS combination. A similar synergistic interaction was confirmed in TNBC cells, with CI values of 0.713 and 0.806, respectively (Table 5).

Angiogenesis mediator

The anti-angiogenic evaluation demonstrated that the niosomal MEF combined with cisplatin exhibited superior inhibitory effects on VEGF and KDR expression across both cell lines. ELISA and qPCR analyses revealed strong concordance between protein and mRNA level measurements. Radar plot visualization distinctly highlighted the enhanced efficacy of this combination treatment compared to other groups, with all angiogenesis-related indicators showing marked improvement. Notably, the nanoformulation of MEF in combination with cisplatin displayed significantly greater potency than its free form, likely attributable to the unique pharmacokinetic advantages of the nano-delivery system. The differential response observed between TNBC and MCF-7 cells underscores the particular therapeutic potential of this approach for TNBC. These findings robustly support the enhanced anti-angiogenic efficacy achieved through nanoformulation-mediated co-delivery, which effectively targets multiple angiogenesis pathways simultaneously (Figs. 7 and 10A).

Apoptotic mediator

The quantitative analysis of apoptotic mediators revealed significant alterations in gene expression and protein levels following treatment with cisplatin (CIS), mefloquine (MEF), niosomal mefloquine (NMEF), and their combinations (MEF + CIS and NMEF + CIS) compared to the untreated control (UC). Real-time PCR and ELISA results demonstrated a marked upregulation of pro-apoptotic markers, including BAX, CASP3, and CASP7, alongside a downregulation of the anti-apoptotic protein BCL-2 (Figs. 8 and 9). These findings indicate a robust activation of the apoptotic pathway, particularly in response to NMEF and its combination with CIS, suggesting enhanced therapeutic efficacy through targeted induction of apoptosis. The data underscore the potential of NMEF as a promising agent for apoptosis-mediated cancer therapy. To visually summarize the modulation of apoptotic markers across treatments, additional normalized radar plots were created using ELISA and Real-Time PCR data. These plots, positioned alongside Figs. 8 and 9 respectively, maintain a unified gene layout (BCL-2 at the top, BAX at the bottom, CASP3 on the right, and CASP8 on the left). They clearly illustrate the consistent downregulation of BCL-2 and upregulation of pro-apoptotic genes, especially BAX and CASP3, in the CIS-NMEF group. The aligned patterns across both protein and gene expression levels further confirm the synergy and mechanistic consistency of this combination therapy in enhancing apoptosis (Fig. 10C and D).

ROS production

The impact of MEF (both free and niosomal forms), CIS, and their combinations on ROS production was evaluated in treated MCF-7 and TNBC cells compared to the control group. The results demonstrated a significant increase ($P < 0.001$) in ROS levels in both cell lines following treatment with MEF, CIS, and their combinations, with the highest ROS production observed in the CIS-NMEF group. This indicates that the treatments effectively induce oxidative stress, a key mechanism underlying their cytotoxic effects. The niosomal formulation of MEF further enhanced ROS generation, likely due to improved cellular uptake and sustained drug release, reinforcing its potential as a chemosensitizer in combination therapy (Fig. 11).

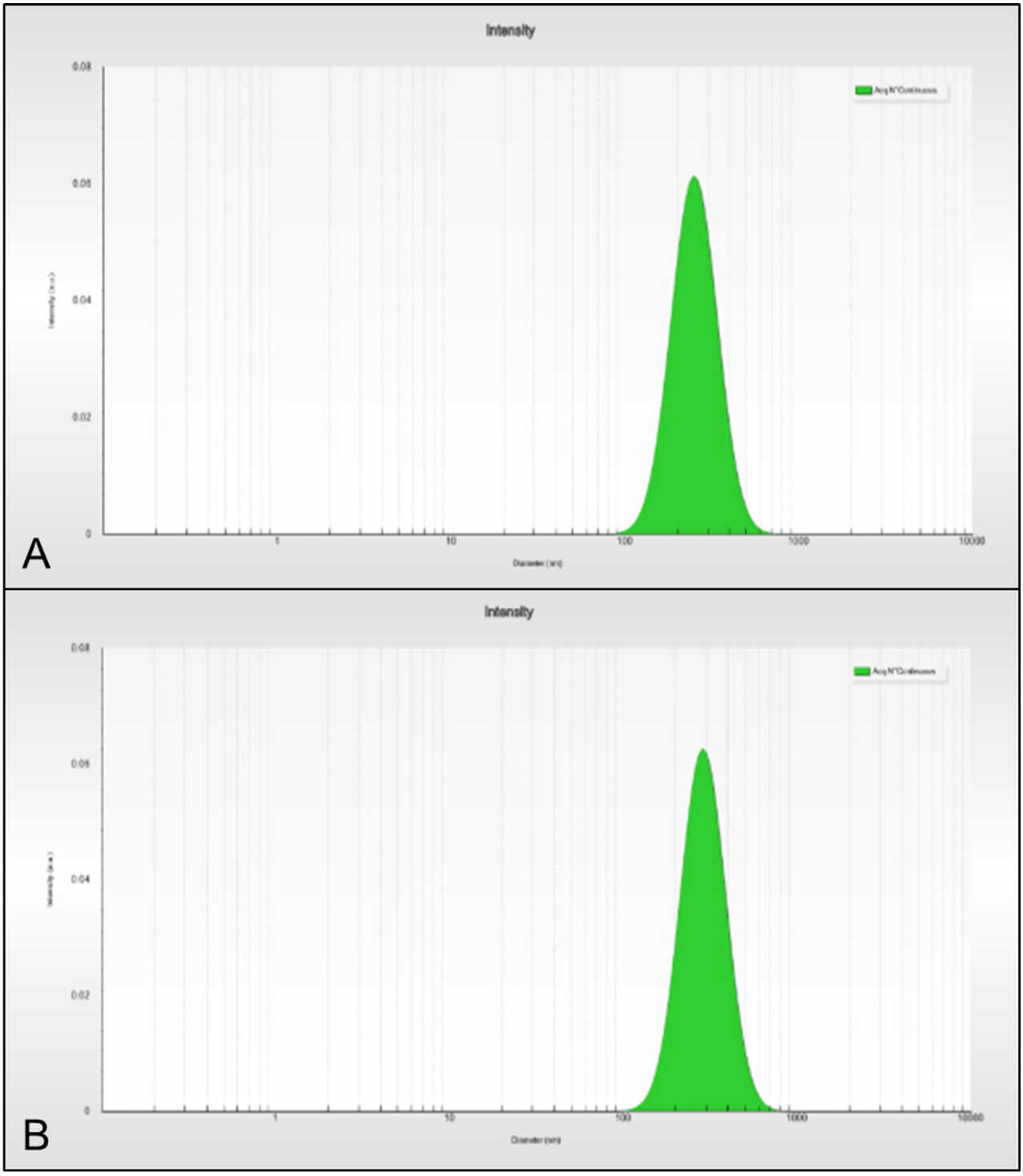

Fig. 5 Vesicle size distribution diagram of MEF niosomes at one week (**A**) and six months (**B**) post-preparation. The similarity in the bell-shaped distribution pattern over this period demonstrates the excellent physical stability of the niosomal formulation over time

Table 3 Vesicle size, PDI, and EE% of Niosomal formulation during storage at 4–8 °C

Formulation	Z average (nm)				PDI				EE%
	1 Week	1 Month	3 Months	6 Months	1 Week	1 Month	3 Months	6 Months	
MEF Niosomes	218.02	209.11	244.02	251.06	0.277	0.211	0.241	0.221	87.21 ± 1.30

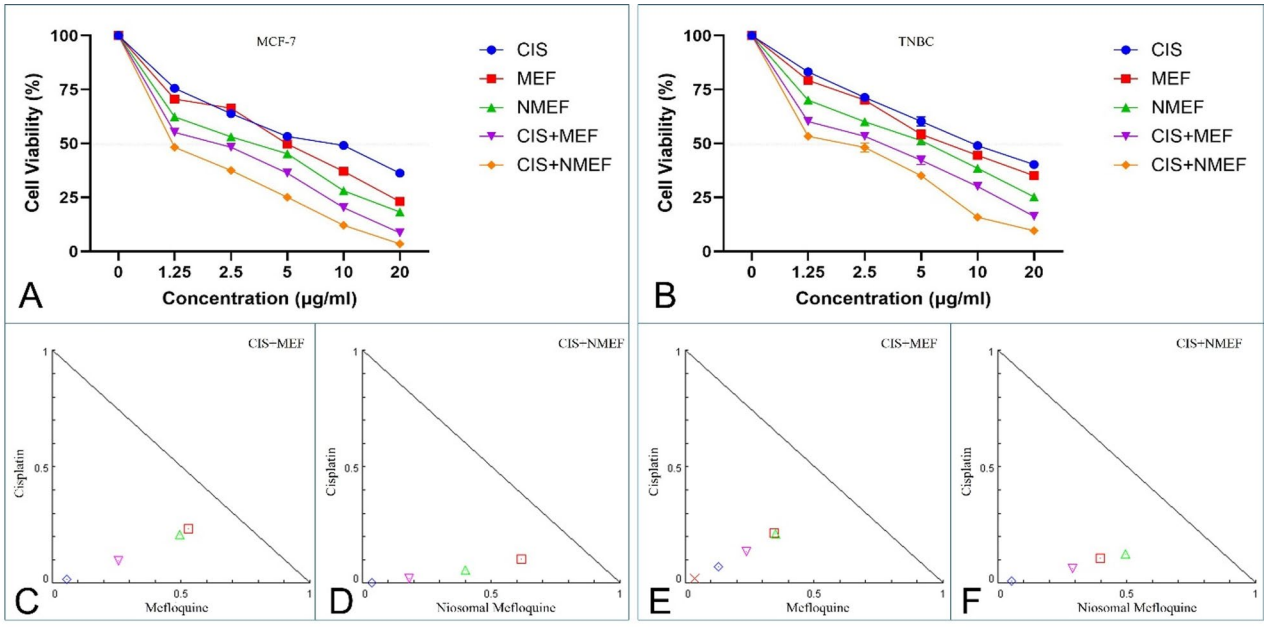

Fig. 6 **A**, **B** Cell viability of MCF-7 (**A**) and TNBC (**B**) cells treated with varying concentrations (1.25–20 µg/ml) of Cisplatin (CIS), Mefloquine (MEF), Niosomal Mefloquine (NMEF), and their combinations (CIS-MEF, CIS-NMEF) for 48 h. Data indicate enhanced cytotoxicity for combination treatments, particularly CIS-NMEF. **C**–**F** Isobologram analysis of drug combinations in MCF-7 (**C**, **D**) and TNBC (**E**, **F**) cells. Plots demonstrate synergistic effects, with data points below the line of additivity for both CIS-MEF and CIS-NMEF treatments

Table 4 Cytotoxicity of cisplatin, mefloquine, Niosomal mefloquine and combination of in MCF-7 and TNBC cell lines and selective index (SI)

Drug Formulation	IC 50 (µg/ml) MCF-7	CC 50 (µg/ml) TNBC	Selective Index (SI) *
Cisplatin	6.29 ± 0.21	9.72 ± 0.84	1.54
Mefloquine	4.47 ± 1.8	6.41 ± 0. 11	1.43
Niosomal Mefloquine	2.96 ± 0.38	4.40 ± 0.32	1.37
Mefloquine + Cisplatin	2.33 ± 0.27	2.76 ± 0.27	1.18
Cisplatin + Niosomal Mefloquine	1.78 ± 0.47	2.30 ± 0.83	1.29

• SI = CC50/IC50

Table 5 Combination index (CI) values for drug combinations in MCF-7 and TNBC cell lines at different effect levels (Fa)

Cell Line	Drug Combination	Fa = 0.50 (IC50)	Fa = 0.75	Fa = 0.90	Interpretation
MCF-7	Mefloquine + Cisplatin	0.892	0.815	0.764	Synergism
	Niosomal MEF + Cisplatin	0.883	0.791	0.728	Synergism
TNBC	Mefloquine + Cisplatin	0.713	0.659	0.612	Strong Synergism
	Niosomal MEF + Cisplatin	0.806	0.743	0.697	Synergism

Discussion

Despite progress in breast cancer therapy, TNBC remains one of the most aggressive and treatment-resistant subtypes due to its lack of hormone receptors and high metastatic potential [30]. Angiogenesis plays a critical role in TNBC progression by supplying nutrients and oxygen [31], while evasion of apoptosis supports tumor survival and resistance to conventional therapies [32]. Consequently, targeting both angiogenesis and apoptosis presents a promising strategy for developing more effective treatments [33].

MEF, an established antimalarial agent, has recently drawn attention for its anticancer properties, including anti-angiogenic activity, lysosomal disruption, ROS generation, and induction of mitochondrial-mediated apoptosis [16, 21, 34, 35]. These multifaceted effects make MEF a strong candidate for drug repurposing in oncology, particularly in combination with standard chemotherapeutics, such as CIS. CIS, a platinum-based drug, induces DNA damage and apoptosis but is often limited by systemic toxicity and drug resistance, prompting interest in combination regimens that can enhance efficacy and reduce side effects [36, 37].

In this study, we investigated the therapeutic potential of MEF both in free and NMEFalone and in combination with CIS in MCF-7 and TNBC cell lines. Results showed that co-administration, particularly CIS-NMEF, led to synergistic increases in cytotoxicity, angiogenesis inhibition, and apoptosis induction. Molecular

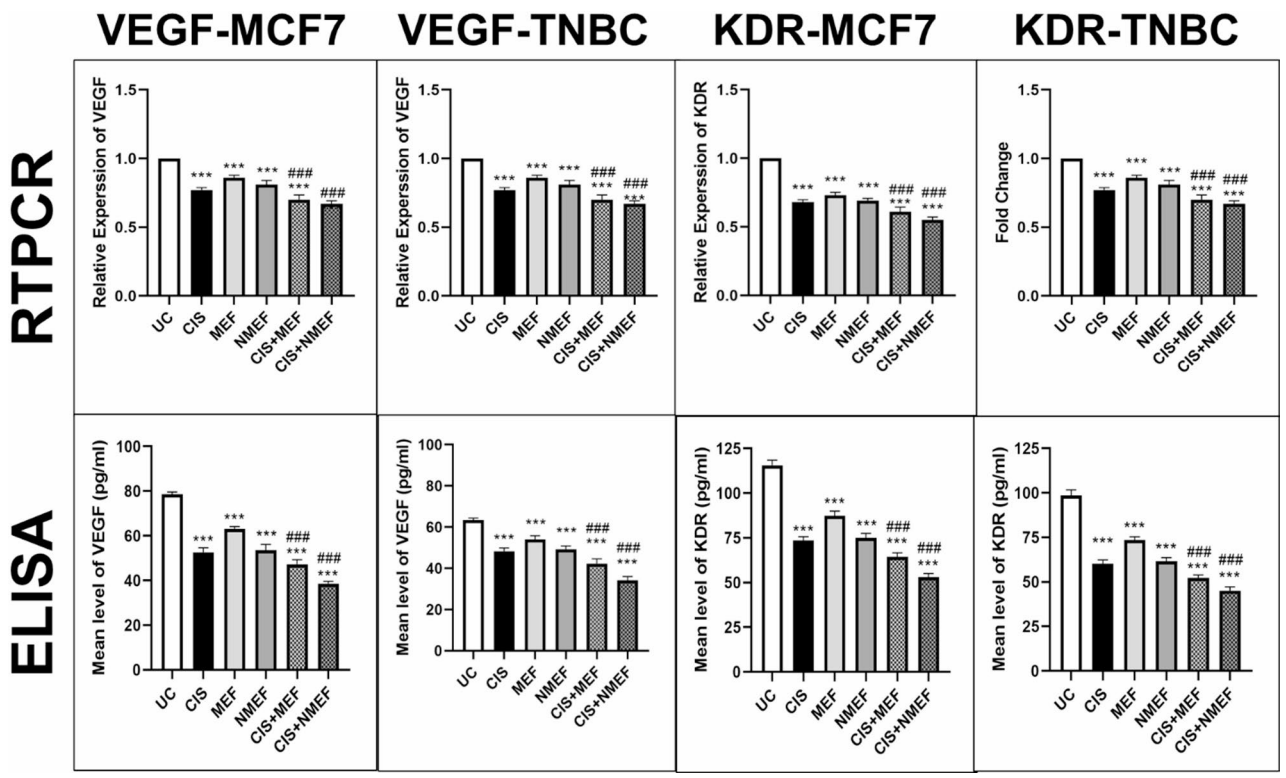

Fig. 7 Effect of Cisplatin (CIS), mefloquine (MEF), niosomal mefloquine (NMEF), and combination (MEF + CIS and CIS + NMEF) on gene expression and mean level of angiogenetic mediators (VEGF, KDR), (*** in comparison with UC ($P < 0.001$))(### comparassion between single theraphy and combination ($P < 0.001$))

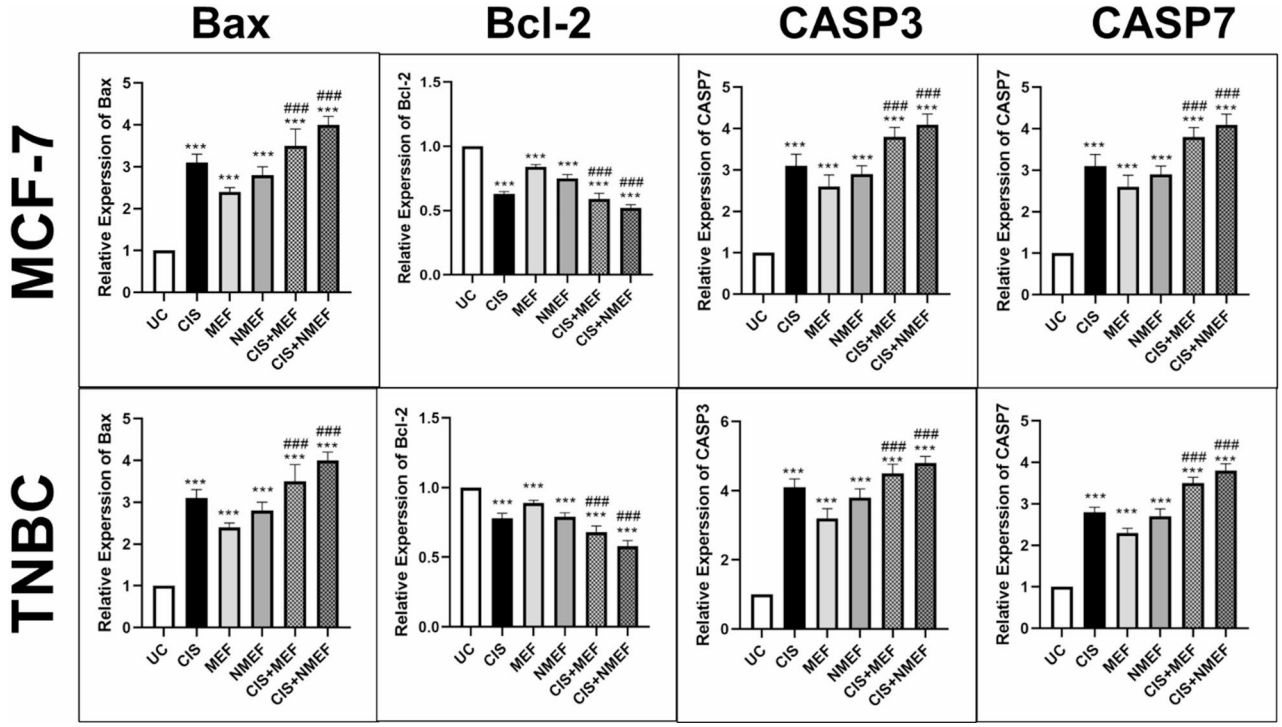

Fig. 8 Effect of Cisplatin (CIS), mefloquine (MEF), niosomal mefloquine (NMEF) and combination (MEF + CIS and NMEF + CIS) on gene expression of apoptotic mediators (Bax, Bcl-2, CASP3 and CASP8), (*** in comparison with UC ($P < 0.001$))(### comparassion between single theraphy and combination ($P < 0.001$))

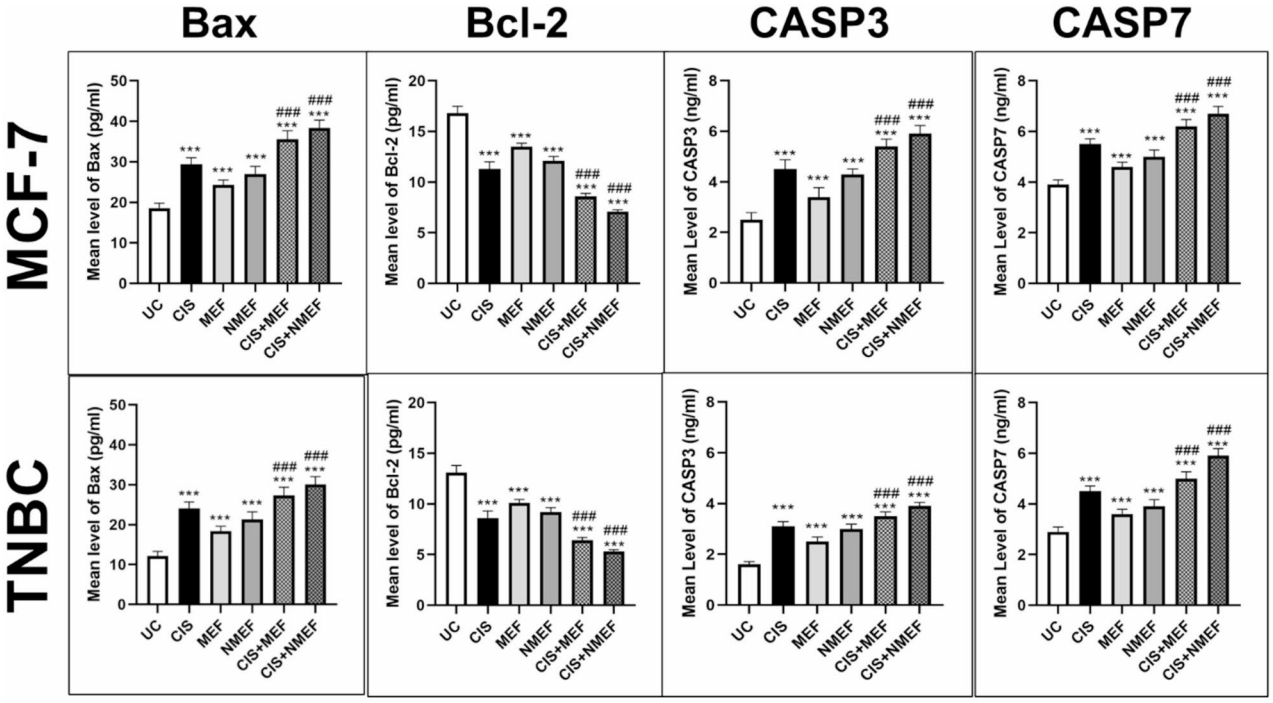

Fig. 9 Effect of Cisplatin (CIS), mefloquine (MEF), niosomal mefloquine (NMEF), and combination (MEF + CIS and NMEF + CIS) on mean level of apoptotic mediators (Bax, Bcl-2, CASP3, and CASP8), (*** in comparison with UC ($P < 0.001$))(### comparassion between single theraphy and combination ($P < 0.001$))

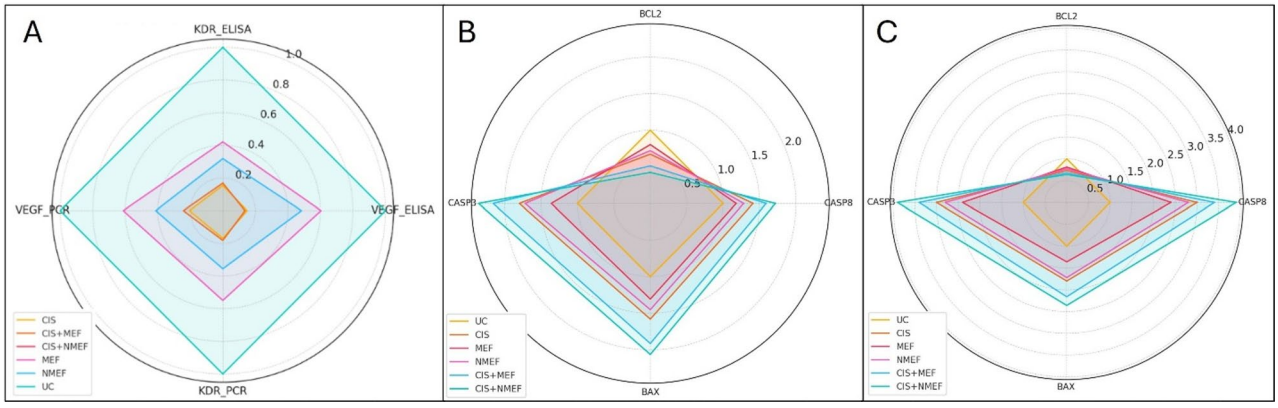

Fig. 10 Effect of Cisplatin (CIS), mefloquine (MEF), niosomal mefloquine (NMEF), and their combinations (MEF + CIS and NMEF + CIS) on (**A**) angiogenesis mediators (VEGF, KDR) (corresponding to Fig. 7), (**B**) apoptotic gene expression (Bax, Bcl-2, CASP3, CASP8) (corresponding to Fig. 8), and (**C**) apoptotic protein levels (Bax, Bcl-2, CASP3, CASP8) (corresponding to Fig. 9). Data demonstrate the synergistic modulation of key pathways by combination treatments, particularly NCIS-MEF

docking revealed that MEF had higher binding affinities to pro- and anti-apoptotic proteins (BAX, Bcl-2) and VEGFR than CIS [38]. The niosomal formulation further improved binding, likely due to enhanced stability and receptor engagement [16].

NMEF exhibited favorable physicochemical properties—stable vesicle size (~ 218 nm), low polydispersity, and high encapsulation efficiency (>87%)—that were maintained over six months, supporting its suitability for tumor targeting via the Enhanced Permeability and Retention (EPR) effect [39]. These characteristics contribute to improved delivery and sustained release in tumor tissues. Similar findings have been reported in other studies where niosomal encapsulation improved drug efficacy and reduced cancer cell invasiveness [23, 40–42].

Cytotoxicity assays demonstrated that both MEF and CIS reduced cancer cell viability in a dose-dependent manner, with stronger effects when combined. Notably, the CIS-NMEF group showed the lowest IC50 values and the strongest synergy (combination index < 1). This potent synergistic effect (CI < 1) is of high clinical

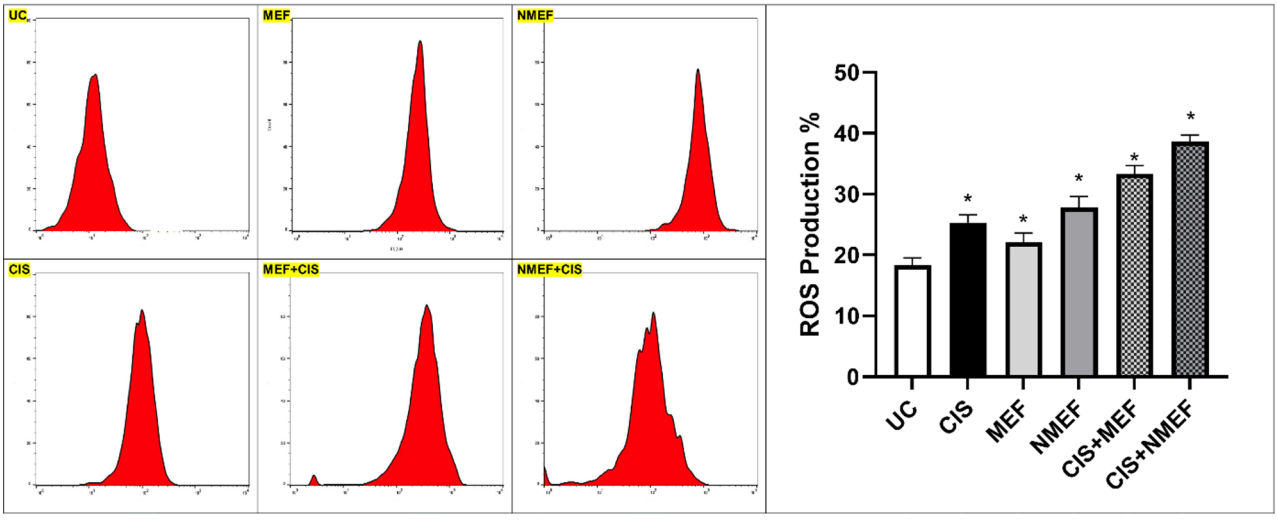

Fig. 11 Effect of Cisplatin (CIS), mefloquine (MEF), niosomal mefloquine (NMEF) and combination (CIS-MEF + and NCIS-MEF) on ROS production in comparassion UC (*$P < 0.001$)

importance as it allows for a reduction in drug dosage, a concept described by the Dose Reduction Index (DRI). Our results imply that to achieve a certain level of cell inhibition, a significantly lower dose of each drug is required in the combination therapy compared to the monotherapy. This dose reduction could substantially mitigate the severe side effects and systemic toxicity associated with cisplatin, such as nephrotoxicity and neurotoxicity, ultimately improving patient tolerance to the treatment. The Selectivity Index (SI) was used in this study as an internal comparison of toxicity between the highly aggressive TNBC cell line and the less aggressive MCF-7 line. Since a normal cell line was not tested, these results do not claim a lack of toxicity to normal cells; rather, an SI value above 1 suggests a higher selective toxicity towards the more aggressive TNBC cancer cell line, which is a promising finding. These results indicate that the nanoformulation enhances drug potency and selectivity, particularly against aggressive TNBC cells.

Gene expression analysis confirmed activation of the intrinsic apoptotic pathway following co-treatment. CIS-NMEF led to marked upregulation of *BAX*, *CASP3*, and *CASP7*, along with significant downregulation of Bcl-2. The increased BAX/Bcl-2 ratio supports mitochondrial-mediated apoptosis and correlates with reduced cell viability. These effects were more pronounced with the niosomal MEF formulation, reinforcing its role in amplifying CIS's pro-apoptotic activity. These findings are consistent with prior studies demonstrating MEF's ability to induce apoptosis via caspase activation and Bcl-2 downregulation in breast cancer cell lines, including T47D and MDA-MB-231 [22].

Simultaneously, real-time PCR and ELISA revealed significant downregulation of angiogenesis-related genes VEGF and KDR at both mRNA and protein levels in cells treated with CIS-NMEF. This dual-level inhibition is crucial for suppressing tumor vascularization, particularly in highly angiogenic TNBC cells. The enhanced anti-angiogenic effect likely stems from improved cellular uptake and prolonged molecular interactions enabled by the NMEF. These results align with prior research in glioblastoma models, where MEF inhibited microvascular endothelial differentiation and angiogenesis through lysosomal destabilization and oxidative stress, ultimately suppressing tumor vascularization [16].

The docking results demonstrated strong binding affinities of MEF and CIS to BAX, Bcl-2, and VEGFR, with MEF showing superior interaction compared to CIS. The CIS-NMEF further enhanced binding, particularly with VEGFR (– 139.19) and Bcl-2 (– 136.09), suggesting improved receptor targeting via nanocarrier delivery. These findings are consistent with the in vitro upregulation of pro-apoptotic and downregulation of angiogenic markers.

Interestingly, our results align with those of our previous study, which also employed molecular docking to evaluate the interactions of bioactive compounds with BAX, Bcl-2, and VEGFR [38, 43]. In this study, the best-performing phytochemicals exhibited MolDock scores within a similar range and disrupted the anti-apoptotic Bcl-2 activity while promoting BAX interaction. Like our findings, strong VEGFR binding was correlated with anti-angiogenic activity. However, our study extends this by demonstrating that co-delivery in a niosomal system improves binding affinity and likely bioavailability, providing a more targeted and synergistic anticancer strategy.

These results support the hypothesis that nanoformulated MEF enhances the therapeutic potential of CIS by promoting apoptosis and inhibiting angiogenesis, as

demonstrated in both molecular docking and cellular assays. Further in vivo validation is needed to confirm these interactions in a physiological context.

Functional assays further supported these findings, showing increased ROS generation and decreased viability in cells treated with MEF and CIS, especially in the CIS-NMEF group. This aligns with prior research indicating MEF's ability to disrupt mitochondrial function and activate apoptotic cascades via oxidative stress [19, 21, 44].

This study demonstrates that combining MEF with CIS especially in its niosomal form—effectively induces apoptosis and inhibits angiogenesis in breast cancer cells, offering a promising strategy for treating aggressive subtypes like TNBC. The niosomal formulation enhances MEF's bioavailability and intracellular delivery, increasing its chemosensitizing potential. However, the findings are based solely on in silico modeling and in vitro experiments using cancer cell lines, which lack the complexity of the in vivo tumor microenvironment, including immune interactions and systemic responses, as demonstrated in the previous chick embryo model [43, 45]. Furthermore, critical aspects such as the long-term safety, pharmacokinetics, and biodistribution of the NMEF formulation remain untested. These limitations underscore the need for comprehensive in vivo studies to validate the therapeutic potential, optimize dosing strategies, and assess the clinical translatability of the CIS-MEF combination.

Abbreviations

CIS	Cisplatin
CI	Combination index
DMEM	Dulbecco's modified eagle medium
EE	Encapsulation efficiency
ELISA	Enzyme-linked immuno_sorbent assay
FBS	Fetal bovine serum
TFR	Flow rate
FRR	Flow rate ratio
IC50	Inhibitory concentrations
MEF	Mefloquine
NMEF	Niosomal mefloquine
NF-κB	Nuclear factor kappa
OD	Optical density
PBS	Phosphate-buffered saline
PDI	Polydispersity index
qPCR	quantitative real-time pcr
ROS	Reactive oxygen species
SI	Selective index
TNBC	Triple-negative breast cancer
VEGF	Vascular endothelial growth factor
KDR	Vascular endothelial growth factor receptor

Acknowledgements
We would like to thank all the personnel of the Leishmaniasis Research Center for their help in conducting this study.

Authors' contributions
ZS and AR (conceived and designed the experiment), EM (in silico modeling), ES, AK, GM, MKh (Metdologist and performed the experiment), MARE (Prepration noisome form of drugs), AKh, ES (wrote the manuscript). SS, GM and MZ (reviewed and revised the manuscript). All authors read and approved the final manuscript.

Funding
This work was supported by the Kerman University of Medical Sciences (Prokect no. 403000093).

Data availability
The datasets used and analyzed during the current study are available from the corresponding author.

Declarations

Ethics approval and consent to participate
This study was approved by the Research Ethics Committees of Afzalipour Hospital, Kerman University of Medical Sciences (Approval ID: IR.KMU.AH.REC.1403.149).

Consent for publication
Not applicable.

Competing interests
The authors declare no competing interests.

Abbreviations.
- Cisplatin (CIS).
- Combination Index (CI).
- Dulbecco's Modified Eagle Medium (DMEM).
- Encapsulation Efficiency (EE).
- Enzyme-linked immuno_sorbent assay (ELISA).
- Fetal Bovine Serum (FBS).
- Flow Rate (TFR).
- Flow Rate Ratio (FRR).
- Inhibitory Concentrations (IC50).
- Mefloquine (MEF).
- Niosomal Mefloquine (NMEF).
- Nuclear Factor kappa B (NF-κB).
- Optical Density (OD).
- Phosphate-Buffered Saline (PBS).
- Polydispersity Index (PDI).
- quantitative Real-Time PCR (qPCR).
- Reactive Oxygen Species (ROS).
- Selective Index (SI).
- Triple-Negative Breast Cancer (TNBC).
- Vascular Endothelial Growth Factor (VEGF).
- Vascular Endothelial Growth Factor Receptor (KDR).

Author details
[1]Obstetrics and Gynecology Center, Afzalipour School of Medicine, Kerman University of Medical Sciences, Kerman, Iran
[2]Leishmaniasis Research Center, Kerman University of Medical Sciences, Kerman, Iran
[3]School of Dentistry, Tehran University of Medical Sciences, Tehran, Iran
[4]Pharmaceutics Research Center, Institute of Pharmaceutical Sciences, Kerman University of Medical Sciences, Kerman, Iran

Received: 26 August 2025 / Accepted: 19 November 2025
Published online: 26 November 2025

References

1. Siegel RL, Miller KD, Wagle NS, Jemal A. Cancer statistics, 2023. Cancer J Clin. 2023;73(1):17–48.
2. Bonotto M, Gerratana L, Poletto E, Driol P, Giangreco M, Russo S, et al. Measures of outcome in metastatic breast cancer: insights from a real-world scenario. Oncologist. 2014;19(6):608–15.
3. Kumar P, Aggarwal R. An overview of triple-negative breast cancer. Arch Gynecol Obstet. 2016;293:247–69.
4. Wang S, Guo S, Guo J, Du Q, Wu C, Wu Y, et al. Cell death pathways: molecular mechanisms and therapeutic targets for cancer. MedComm. 2024;5(9):e693.

5. Wang S, Chen X, Zhang X, Wen K, Chen X, Gu J, et al. Pro-apoptotic gene BAX is a pan-cancer predictive biomarker for prognosis and immunotherapy efficacy. Aging. 2024;16(14):11289–317.
6. Zhang Q, Liu X, Wei Q, Xiong S, Luo W, Zhou Y, et al. Apoptotic breast cancer cells after chemotherapy induce pro-tumour extracellular vesicles via LAP-competent macrophages. Redox Biol. 2025;80:103485.
7. Ye F, Dewanjee S, Li Y, Jha NK, Chen ZS, Kumar A, et al. Advancements in clinical aspects of targeted therapy and immunotherapy in breast cancer. Mol Cancer. 2023;22(1):105.
8. Florea A-M, Büsselberg D. Cisplatin as an anti-tumor drug: cellular mechanisms of activity, drug resistance and induced side effects. Cancers. 2011;3(1):1351–71.
9. Ramer R, Schmied T, Wagner C, Haustein M, Hinz B. The antiangiogenic action of cisplatin on endothelial cells is mediated through the release of tissue inhibitor of matrix metalloproteinases-1 from lung cancer cells. Oncotarget. 2018;9(75):34038–55.
10. Zhou J, Kang Y, Chen L, Wang H, Liu J, Zeng S, et al. The drug-resistance mechanisms of five platinum-based antitumor agents. Front Pharmacol. 2020;11:343.
11. Ho AN, Kiesel VA, Gates CE, Brosnan BH, Connelly SP, Glenny EM, et al. Exogenous metabolic modulators improve response to carboplatin in Triple-Negative breast cancer. Cells. 2024;13(10):806.
12. Berg AL, Rowson-Hodel A, Wheeler MR, Hu M, Free S, Carraway KL III. Engaging the lysosome and lysosome-dependent cell death in cancer. In: Exon Publications; 2022;195–230. https://doi.org/10.36255/exon-publications-breast-cancer-lysosome.
13. Weiss WR, Oloo AJ, Johnson A, Koech D, Hoffman SL. Daily primaquine is effective for prophylaxis against falciparum malaria in Kenya: comparison with mefloquine, doxycycline, and chloroquine plus proguanil. J Infect Dis. 1995;171(6):1569–75.
14. Farrar J, Hotez PJ, Junghanss T, Kang G, Lalloo D, White NJ, et al. Manson's Tropical Diseases E-Book. Elsevier health sciences; 2023. https://www.sciencedirect.com/book/9780702079597/mansons-tropical-diseases.
15. Wong W, Bai X-C, Sleebs BE, Triglia T, Brown A, Thompson JK, et al. Mefloquine targets the plasmodium falciparum 80S ribosome to inhibit protein synthesis. Nat Microbiol. 2017;2(6):1–9.
16. Wan B, Wu Z, Zhang X, Huang B. Mefloquine as a dual inhibitor of glioblastoma angiogenesis and glioblastoma via disrupting lysosomal function. Biochem Biophys Res Commun. 2021;580:7–13.
17. Xiang W, Lam YH, Sng C, Cheong MA, Than H, Hwang WY, et al. Mefloquine effectively targets blast phase chronic myeloid leukemia through inducing oxidative stress and lysosomal disruption. In.: American Society of Hematology Washington, DC; 2016. https://doi.org/10.1182/blood.V128.22.5426.5426.
18. Suski JM, Lebiedzinska M, Bonora M, Pinton P, Duszynski J, Wieckowski MR. Relation between mitochondrial membrane potential and ROS formation. In: Mitochondrial Bioenergetics: Methods Protocols. 2012;183–205. https://doi.org/10.1007/978-1-61779-382-0_12.
19. Yan K-H, Yao C-J, Hsiao C-H, Lin K-H, Lin Y-W, Wen Y-C, et al. Mefloquine exerts anticancer activity in prostate cancer cells via ROS-mediated modulation of Akt, ERK, JNK and AMPK signaling. Oncol Lett. 2013;5(5):1541–5.
20. Liu Y, Chen S, Xue R, Zhao J, Di M. Mefloquine effectively targets gastric cancer cells through phosphatase-dependent inhibition of PI3K/Akt/mTOR signaling pathway. Biochem Biophys Res Commun. 2016;470(2):350–5.
21. Xu X, Wang J, Han K, Li S, Xu F, Yang Y. Antimalarial drug mefloquine inhibits nuclear factor kappa B signaling and induces apoptosis in colorectal cancer cells. Cancer Sci. 2018;109(4):1220–9.
22. Sharma N, Thomas S, Golden EB, Hofman FM, Chen TC, Petasis NA, et al. Inhibition of autophagy and induction of breast cancer cell death by mefloquine, an antimalarial agent. Cancer Lett. 2012;326(2):143–54.
23. Estabragh MAR, Behnam B, Torkzadeh-Mahani M, Pardakhty A. Niosome as a drug delivery carrier for sorafenib: preparation, investigation of physicochemical properties, and in vitro effects on HepG2 cell line. Adv Pharm Bull. 2024;14(4):836.
24. Estabragh MAR, Pardakhty A, Ahmadzadeh S, Dabiri S, Afshar RM, Abbasi MF. Successful application of alpha lipoic acid niosomal formulation in cerebral ischemic reperfusion injury in rat model. Adv Pharm Bull. 2021;12(3):541.
25. Obeid MA, Elburi A, Young LC, Mullen AB, Tate RJ, Ferro VA. Formulation of nonionic surfactant vesicles (NISV) prepared by microfluidics for therapeutic delivery of SiRNA into cancer cells. Mol Pharm. 2017;14(7):2450–8.
26. Obeid MA, Khadra I, Aljabali AA, Amawi H, Ferro VA. Characterisation of niosome nanoparticles prepared by microfluidic mixing for drug delivery. International Journal of Pharmaceutics: X. 2022;4:100137.
27. Ritwiset A, Krongsuk S, Johns JR. Molecular structure and dynamical properties of niosome bilayers with and without cholesterol incorporation: a molecular dynamics simulation study. Appl Surf Sci. 2016;380:23–31.
28. Pelalak R. Molecular dynamics simulation of novel diamino-functionalized Hollow mesosilica spheres for adsorption of dyes from synthetic wastewater. J Mol Liq. 2021;322:114812.
29. Rao AB, Murthy R. A rapid spectrophotometric method for the determination of mefloquine hydrochloride. J Pharm Biomed Anal. 2002;27(6):959–65.
30. Lee A, Djamgoz MBA. Triple negative breast cancer: emerging therapeutic modalities and novel combination therapies. Cancer Treat Rev. 2018;62:110–22.
31. Lee SH, Jeong D, Han YS, Baek MJ. Pivotal role of vascular endothelial growth factor pathway in tumor angiogenesis. Ann Surg Treat Res. 2015;89(1):1–8.
32. Ferrari P, Scatena C, Ghilli M, Bargagna I, Lorenzini G, Nicolini A. Molecular mechanisms, biomarkers and emerging therapies for chemotherapy resistant TNBC. Int J Mol Sci. 2022. https://doi.org/10.3390/ijms23031665.
33. Mou J, Li C, Zheng Q, Meng X, Tang H. Research progress in tumor angiogenesis and drug resistance in breast cancer. Cancer Biol Med. 2024;21(7):571–85.
34. Mereddy G, Ronayne C. Repurposing antimalarial drug mefloquine for cancer treatment. Transl Med (Sunnyvale). 2018;8(199):2161–10251000199.
35. Lam Yi H, Than H, Sng C, Cheong MA, Chuah C, Xiang W. Lysosome Inhibition by mefloquine preferentially enhances the cytotoxic effects of tyrosine kinase inhibitors in blast phase chronic myeloid leukemia. Transl Oncol. 2019;12(9):1221–8.
36. Ali R, Aouida M, Alhaj Sulaiman A, Madhusudan S, Ramotar D. Can cisplatin therapy be improved? Pathways that can be targeted. Int J Mol Sci. 2022. https://doi.org/10.3390/ijms23137241.
37. Li Q, Chen S, Wang X, Cai J, Huang H, Tang S, et al. Cisplatin-based combination therapy for enhanced cancer treatment. Curr Drug Targets. 2024;25(7):473–91.
38. Salari Z, Khosravi A, Pourkhandani E, Molaakbari E, Salarkia E, Keyhani A, et al. The inhibitory effect of 6-gingerol and cisplatin on ovarian cancer and antitumor activity: in silico, in vitro, and in vivo. Front Oncol. 2023;13:1098429.
39. Vagena I-A, Malapani C, Gatou M-A, Lagopati N, Pavlatou EA. Enhancement of EPR effect for passive tumor targeting: current status and future perspectives. Appl Sci. 2025;15(6):3189.
40. Bashkeran T, Kamaruddin AH, Ngo TX, Suda K, Umakoshi H, Watanabe N, et al. Niosomes in cancer treatment: a focus on curcumin encapsulation. Heliyon. 2023. https://doi.org/10.1016/j.heliyon.2023.e18710.
41. Sharafshadeh MS, Tafvizi F, Khodarahmi P, Ehtesham S. Preparation and physicochemical properties of cisplatin and doxorubicin encapsulated by niosome alginate nanocarrier for cancer therapy. Int J Biol Macromol. 2023;235:123686.
42. Dabbagh Moghaddam F, Akbarzadeh I, Marzbankia E, Farid M, Khaledi L, Reihani AH, et al. Delivery of melittin-loaded niosomes for breast cancer treatment: an in vitro and in vivo evaluation of anti-cancer effect. Cancer Nanotechnol. 2021;12(1):14.
43. Khosravi A, Sharifi I, Tavakkoli H, Molaakbari E, Bahraminegad S, Salarkia E, et al. Cytotoxicity of amphotericin B and ambisome: in silico and in vivo evaluation employing the chick embryo model. Front Pharmacol. 2022;13:860598.
44. Mudassar F, Shen H, O'Neill G, Hau E. Targeting tumor hypoxia and mitochondrial metabolism with anti-parasitic drugs to improve radiation response in high-grade gliomas. J Exp Clin Cancer Res. 2020;39(1):208.
45. Khosravi A, Sharifi I, Tavakkoli H, Keyhani AR, Afgar A, Salari Z, et al. Toxicopathological effects of meglumine antimoniate on human umbilical vein endothelial cells. Toxicol In Vitro. 2019;56:10–8.

Publisher's note